Thermodynamic regulation of ocean warming by cirrus clouds deduced from observations of the 1987 El Niño

V. Ramanathan & W. Collins

Scripps Institution of Oceanography and California Space Institute, University of California at San Diego, La Jolla, California 92093, USA

Observations made during the 1987 El Niño show that in the upper range of sea surface temperatures, the greenhouse effect increases with surface temperature at a rate which exceeds the rate at which radiation is being emitted from the surface. In response to this 'super greenhouse effect', highly reflective cirrus clouds are produced which act like a thermostat, shielding the ocean from solar radiation. The regulatory effect of these cirrus clouds may limit sea surface temperatures to less than 305 K.

WATER vapour and clouds are the dominant regulators of the radiative heating of the planet. General circulation model studies have identified the complex effects of the various cloud and water vapour feedbacks and their importance to climate change[1–3]. We do not understand how these radiative effects respond to a climate change, nor do we understand their feedback effects. What we need is a natural climate-change experiment in a region that exhibits a strong coupling between surface temperatures and radiative fluxes. The tropical Pacific shows such behaviour. In particular, during the El Niño events which occur once every 2–6 years[4], the equatorial Pacific warms by as much as 2–4 K, and the warming is accompanied by marked variations in the radiation fluxes at the top of the atmosphere[5]. Accurate data on the radiation budget from the Earth radiation budget experiment (ERBE)[6] and sea-surface-temperature (SST) data from weather satellites and ships[7] are available for the 1987 El Niño[8]. We use this data set to explore the link between ocean warming and the radiative feedbacks. Relevant definitions are given next.

The total greenhouse effect of the atmosphere and clouds, G, is defined[9] as $G = E - F$, where F is the radiation emitted to space, and $E = \sigma T^4$ is the energy emitted by the ocean surface, with $\sigma = 5.67 \times 10^{-8}$ W m^{-2} K^{-4} and T = SST. Observations of F over the clear-sky regions, F_c, are employed to obtain the atmospheric portion of the greenhouse effect, $G_a = E - F_c$. The difference between G and G_a gives the enhancement of the greenhouse effect caused by clouds, or 'cloud long-wave forcing', $C_l = G - G_a = F_c - F$. Clouds also enhance the albedo (reflectivity) of the planet, thereby decreasing the planetary solar heating. This effect, the 'cloud short-wave forcing' (ref. 6), C_s, is estimated by subtracting the solar energy absorbed by a region from that over just the clear-sky portion of that region. Hence, the absorbed solar energy can be expanded as $S(1-A) = S_c + C_s$, where S is the solar radiation at the top of the atmosphere, A is the column albedo, and S_c is the clear-sky solar absorption. ERBE measurements yield the fluxes for the top of the atmosphere of F, F_c, S and S_c together with the albedo A. Thus we have observable definitions for the various feedback terms.

During the El Niño of 1987, the equatorial Pacific warmed by as much as 3 K (Fig. 1*a*). The warming was accompanied by a significant increase in the greenhouse effect of the atmosphere (Fig. 1*b*) and that of the clouds (Fig. 1*d*). These positive feedback effects are offset by a significant decrease in the absorbed solar energy (Fig. 1*c*). We show that this cirrus regulation of ocean warming is triggered primarily when SSTs exceed 300 K. Results of past studies[9–13] enable us to conclude that the interactions between SST, deep convection, large-scale transport of moisture and cirrus formation are responsible for the observed negative feedback effect of cirrus.

Analyses of the interactions

We begin with the net radiative heating of the surface-atmosphere system, $H = S(1-A) - F$. Adopting the previous definitions for $F = \sigma T^4 - G_a - C_l$ and $S(1-A) = S_c + C_s$, we have

$$H = S_c - \sigma T^4 + G_a + C_l + C_s \quad (1)$$

The absorbed solar radiation, S_c, heats the surface, which emits the energy as long-wave radiation, σT^4. An amount G_a is

TABLE 1 Summary of feedback terms

a, Experiment 1: spatial and seasonal

Domain	Period (month/year)	dG_a/dT (W m^{-2} K^{-1})	dC_s/dC_l
25° N–25° S	4/85	5.6†	−1.07*
	4/87	6.5†	−1.03†
	2/87	6.9†	−0.96*
	2/88	6.3†	−0.94*
10° N–10° S	4/85	7.2†	−1.13*
	4/87	8.1*	−1.12*
	2/87	8.2*	−0.9†
	2/88	8.5†	−0.9†
0–25° N	2/85	4.6*	−1.01*
	4/85	5.2†	−1.26*
0–25° S	2/85	7.4†	−1.03†
	4/85	6.5†	−0.87*
10° N–10° S	4/85; 2/87; 2/88; 4/89	7.7*	−0.95†
Atlantic	Same	7.9*	−1.03†
Indian Ocean	Same	8.1‡	−1.03†

b, Experiment 2: El Niño

Domain	Period (month/year)	dG_a/dT (W m^{-2} K^{-1})	dC_s/dC_l	dC_s/dG	a_s (W m^{-2} K^{-1})	a_l
10° N–10° S	{4/87–4/85; 4/89–4/87; 2/88–2/87}	6.8*	−1.2*	−0.92†	−22‡	18*
	4/87–4/85	9.2*	−1.33†	−0.97*	−20*	16*
	4/89–4/87	8.5*	−1.23†	−0.95†	−19‡	17*
	2/87–2/85	6.4‡	−1.09†	−0.97†		
	2/88–2/87		−1.11*	−0.97*		
	5/87–5/85	8.0*	−1.22†	−0.92†		
	7/87–7/85	5.7*	−1.17†	−0.79‡		
	10/87–10/85	6.0*	−1.32†	−0.99*		

Unless otherwise stated, the domain is the Pacific Ocean stretching from 140° E (western Pacific) to 90° W (eastern Pacific). SST is denoted by T; the atmospheric greenhouse effect by G_a; the cloud long-wave forcing is C_l; the total greenhouse effect is $G = G_a + C_l$; the cloud modulation of absorbed solar energy is the cloud short-wave forcing C_s; and the cloud-forcing slopes a_s (short-wave) and a_l (long-wave) are obtained from Fig. 4*a* and *b*, respectively.

* Correlation coefficient $|r|$ for least-squares linear fit is in range $0.9 > |r| > 0.8$

† $|r| > 0.9$

‡ $0.8 > |r| > 0.7$. When $|r| < 0.7$, the correlation is considered insignificant and is omitted from the table.

trapped in the atmosphere, thus reducing the cooling to space. The long-wave energy flow out of the system is further reduced by the flux C_l trapped in clouds. But this heating effect is offset by the reduction C_s of solar absorption by clouds with $C_s<0$. We wish to examine how G_a, C_l and C_s vary with T. These dependences are obtained both from the spatial and seasonal variations in T and from the 1987 El Niño, which began during late 1986.

We use ERBE measurements for 1985-89. The SSTs are obtained from combined analyses from the National Oceanic and Atmospheric Administration and the National Meteorological Center[7] of satellite and *in situ* data. The data are monthly averaged values with a spatial resolution of 2.5° (latitude) × 2.5° (longitude). The analyses will focus primarily on April, but we will briefly review results for the months of February, May, July and October. April is preferred for several reasons. Because of the near-hemispherical symmetry of solar radiation and of meteorological features in the equatorial regions, we can safely ignore hemispherical asymmetries in the dependence on the solar zenith angle before comparing the albedos of the different oceans. Around April, equatorial SSTs reach peak seasonal values and exceed 300 K over most of the Pacific[4], the minimum SST necessary to initiate deep convection. Finally, the 1987 El Niño warming stabilized at near-maximum values around April 1987.

Experiment 1

In this experiment, we examined spatial variations in the greenhouse effect and cloud forcing for different seasons. The total greenhouse effect $G=G_a+C_l$ increases sharply when the SST exceeds ~300 K (Fig. 2*a*), a feature that is present in all the months and can also be inferred from earlier studies[14,15]. Optically thick cirrus clouds in the upper troposphere are needed to account for the large increase in G of ~100 W m^{-2} as the temperature increases from 300 to 303 K. The slope, dG_a/dT, for the tropical Pacific (10° N to 10° S) is ~6–9 W m^{-2} K^{-1} (Fig. 2*b*, and Table 1), whereas it is ~3.4 W m^{-2} K^{-1} for the entire Pacific (60° N to 60° S). About half of the 3.4 W m^{-2} K^{-1} is due to atmospheric trapping of the increased black-body emission. The balance is due to water vapour feedback[9]: the warmer atmosphere contains more water vapour which in turn traps more radiation. The fact that $dG_a/dT>6$ W m^{-2} K^{-1} has important climate implications.

The surface emission increases at a rate close to $dE/dT=4\sigma T^3\approx 6.1$ W m^{-2} K^{-1} at $\sim T=300$ K. But as $dG_a/dT\geqslant dE/dT$, the energy cannot escape to space but instead is trapped in the atmosphere. Indeed, the slightly larger slope of G_a suggests that the trapping increases faster than the surface emission. The main deduction is that the warmer tropical-ocean/atmosphere system has lost the fundamental negative feedback between temperature and infrared emission which expels excess heat by radiating to space. This tropical 'super greenhouse effect' is caused by a combination of several mutually reinforcing factors, including increases in total-column H_2O[9,10,16]; H_2O continuum absorption[17] which scales quadratically with H_2O partial pressure; higher middle- and upper-troposphere H_2O concentrations[19], and changes in the lapse rate[18,19]. The system is potentially unstable unless another negative feedback exists to stabilize it,

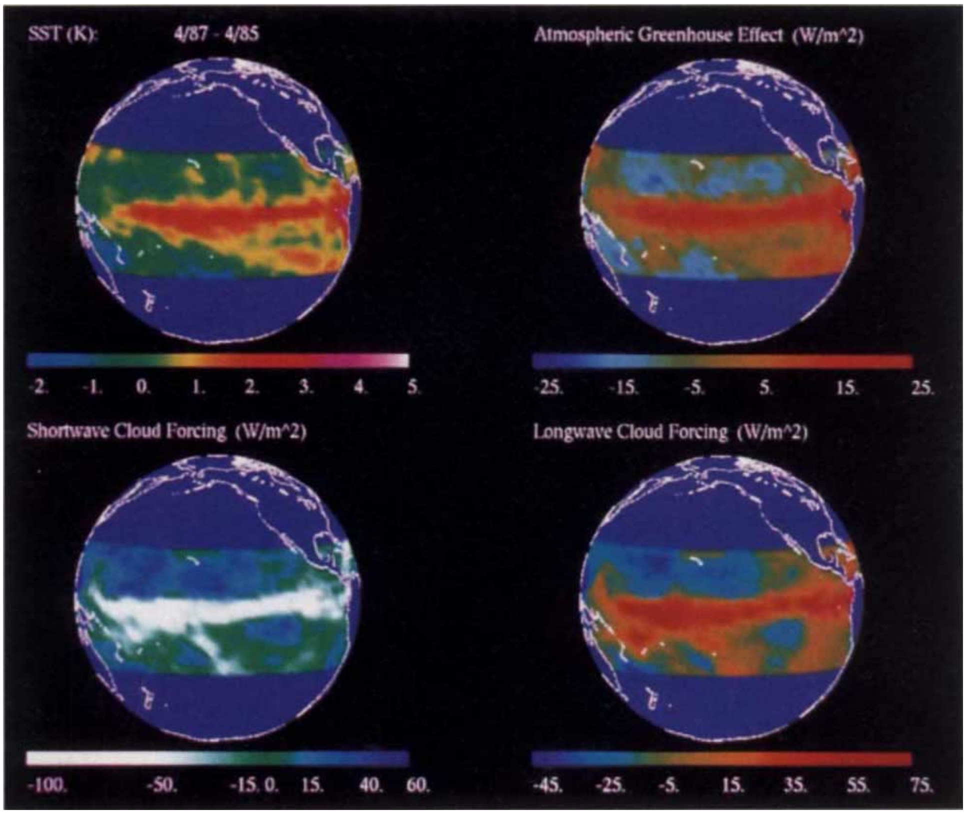

FIG. 1 Changes in the SST, the greenhouse effect and the cloud forcing accompanying the 1987 El Niño. Top left panel (*a*), April 1987 minus April 1985 monthly mean SSTs for 25° N to 25° S. Outside this region changes are much smaller. SST data are obtained from ref. 7. The equatorial warming began during late 1986 and was well established by April of 1987 (ref. 8). Top right panel (*b*), April 1987 minus April 1985 atmospheric greenhouse effect. Bottom left panel (*c*), April 1987 minus April 1985 cloud short-wave forcing. The El Niño warming leads to highly reflective clouds which reduce (as $C_s<0$) the solar energy absorbed by the oceans by as much as 100 W m^{-2}. Bottom right panel (*d*), April 1987 minus April 1985 cloud long-wave forcing, C_l. The greenhouse effect of clouds increases significantly over the regions subject to the surface warming. Increased cirrus cloudiness in the upper troposphere is needed to account for changes in C_l larger than 30 W m^{-2}.

and this brings us to the changes in the cloud forcing. The cloud-forcing terms C_l (Fig. 1*d*) and C_s (Fig. 1*c*) also increase in magnitude for warmer oceans (Fig. 1*a*). A closer examination of the relationship between C_l and C_s (Fig. 2*c*), reveals the strong degree of anti-correlation between the two, which can also be deduced from results published earlier[20-22]. The generality of this finding is shown in Table 1. This remarkable correlation and the fact that large negative values of C_s are correlated with warmer waters (Fig. 1*d*) lead to the following conjecture: as the tropical oceans warm, the rapid rise of G_a with SST leads to an unstable feedback. The warming continues until the clouds become thick enough to shield the ocean from the solar radiation and arrest further warming. This thermostat effect of the cirrus anvils controls the maximum value of SSTs. The validity of this inference is examined next.

Experiment 2

In this experiment, we examined the flux changes that occurred during the 1987 El Niño. The observed changes are very similar to those inferred above. First, G_a increases with SST (Fig. 3*a*) at a rate of 6-9 $\mathrm{W\,m^{-2}\,K^{-1}}$. The plot of dC_s against dC_l (Fig. 3*b*) confirms that clouds with large C_l are also very reflective. As $dC_s/dG \gtrsim -1$, the decrease in the absorbed solar energy nearly balances the increase in the total greenhouse effect (Fig. 3*c*). These results support the inference from experiment 1 that G increases significantly with a warming of the ocean, and this unstable increase is effectively offset by the brighter clouds resulting from the warming. Similar results are obtained for the months of February, May, July and October (Table 1), but results for February and July should be viewed with caution as we have not accounted for seasonal changes in the incoming solar radiation and the solar zenith angle, both of which have complex and largely unknown effects on the cloud-forcing terms.

To probe further into the link between the warming and the absorbed solar energy, we plot the product of dT and dC_s against $(dT)^2$ for each 2.5°×2.5° region (Fig. 4). If the relationship is linear, we can obtain the rate of decrease of C_s with increase in SST from the slope, a_s. A statistically significant relationship does exist for April (Fig. 4 and the column under a_s in Table 1), although it is weaker for the other months; for example, for February 1987 minus February 1985 and for May 1987 minus May 1985, a_s is $\sim -15\ \mathrm{W\,m^{-2}\,K^{-1}}$. The correlation coefficient $|r|$ is only ~0.6 and is almost zero for July and October. But we may obtain a better picture by examining the relationship on a larger scale.

We focus on the region of maximum warming, the central and eastern Pacific from 180° (the date line) to 90° W and 5° N to 5° S. During April, for example, the average SST for this region increased from 300.1 in 1985 to 301.9 K in 1987 and the average C_s changed from −29 in 1985 to $-63\ \mathrm{W\,m^{-2}}$ in 1987 ($dC_s = -34\ \mathrm{W\,m^{-2}}$); for February, SST increases from 299.2 to 301 K and $dC_s = -32\ \mathrm{W\,m^{-2}}$; for May, SST increases from 300 to 301.7 K and $dC_s = -34\ \mathrm{W\,m^{-2}}$; for July, the changes are from 299 to 301 K and $dC_s = -12\ \mathrm{W\,m^{-2}}$; and finally for October, SST increases from 298.6 to 300.3 K and $dC_s = -6\ \mathrm{W\,m^{-2}}$. Several inferences can be made. First, on the larger scale the warming is accompanied by a decrease in solar absorption without exception. This is reassuring as the processes that link SST with C_s involve cooperative interaction between deep convection and the large-scale circulation which transports moisture into the region of warming from the rest of the tropical Pacific (details given later). Second, if we exclude the colder eastern Pacific from 90° W to 120° W, which is mostly devoid of deep convection, dC_s for October decreases from −6 to $-13\ \mathrm{W\,m^{-2}}$ with similar decreases (ranging from −5 to $-9\ \mathrm{W\,m^{-2}}$) during other months. This is another indication of the role of deep convection in triggering the negative feedback between SST and C_s. Finally, the marked decrease of $-dC_s$ towards October, which roughly marks the final phase of the El Niño, is a reminder of the transient nature of the event. As the El Niño warming is

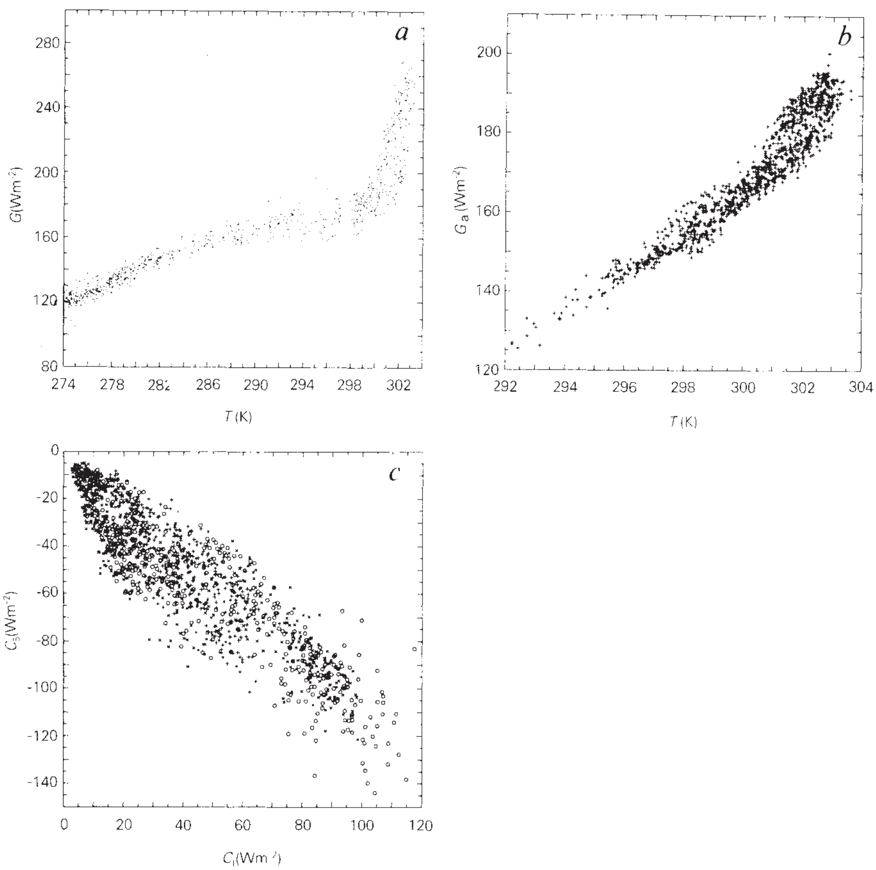

FIG. 2 Monthly mean greenhouse effect and cloud-forcing terms for the Pacific extending from 140° E to 90° W. Each point in this and other figures represents a monthly averaged value for a 2.5° (latitude) × 2.5° (longitude) region. *a*, Total greenhouse effect, *G*, plotted as a function of SST for April 1987 from 85° N to 85° S. Regions with SST < 274 K are excluded. *b*, Atmospheric greenhouse effect G_a against SST for the tropical Pacific from 25° N to 25° S for April 1987. The least-squares linear slope is $dG_a/dT = 6.5\ \mathrm{W\,m^{-2}\,K^{-1}}$ with a correlation coefficient of $r = 0.96$. *c*, Cloud short-wave forcing against cloud long-wave forcing for the region 10° N to 10° S for 4/85(+), 2/87(○), 2/88(×), and 4/87(·). The linear correlation is $dC_s/dC_l = -0.951$ ($r = -0.9$).

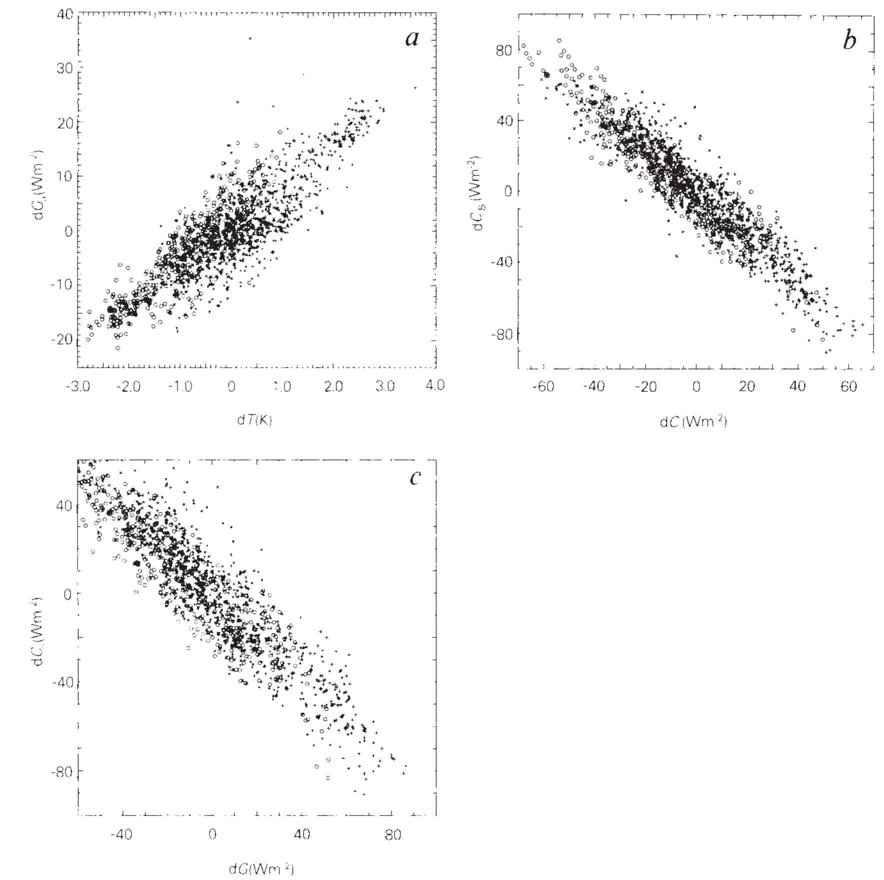

FIG. 3 Changes induced by 1987 El Niño in monthly mean greenhouse effect, cloud-forcing terms and SST for the Pacific ocean (140° E to 90° W) from 10° N to 10° S. The points represent the differences for 4/87 minus 4/85(+), 4/89 minus 4/87(○), and 2/88 minus 2/87(×). *a*, dG_a against dT where d denotes difference between two years. The linear fit is $dG_a/dT = 6.80$ W m^{-2} K^{-1} ($r = 0.85$). *b*, Change in cloud short-wave forcing against change in cloud long-wave forcing. The linear fit is $dC_s/dC_l = -1.20$ ($r = -0.93$). As $dC_s/dC_l < -1$, clouds have a net cooling effect. *c*, Change in cloud short-wave forcing against change in total greenhouse effect $G = G_a + C_l$. The linear fit is $dC_s/dG = -0.92$ ($r = -0.92$), which indicates that the increase in the greenhouse effect is slightly larger than the decrease in solar absorption.

a transient phenomenon which started to revert back to 'normal' conditions around November 1987, considerable changes in the equatorial dynamics during the terminal phase of the El Niño[13] can be expected to modify the radiative feedbacks.

To explore additional climate implications, we estimate the change of C_s with SST, although acknowledging that this is a hazardous task given the nonlinear nature of the coupling between SST, ocean-atmosphere dynamics and radiation physics. We can use two independent methods: (1) From Fig. 3*a*, $dG_a/dT \approx 6.8$ W m^{-2} K^{-1}. As $dC_s = -0.92\,(dC_l + dG_a)$ (Fig. 3*c*) with the further constraint that $dC_s = -1.20\,dC_l$ (Fig. 3*b*), we obtain $dC_s/dT \approx -27$ W m^{-2} K^{-1} and $dC_l/dT \approx 23$ W m^{-2} K^{-1}. (2) The covariance plot (Fig. 4*a*) of dC_s and dT with $(dT)^2$ and the corresponding plot for dC_l (Fig. 4*b*) yield $dC_s/dT \approx -22$ and $dC_l/dT \approx 18$, where because of uncertainties in the SST data, regions with $dT < 1$ K are excluded.

Thermodynamics and dynamics of the feedbacks

In what follows, we describe the fundamental principles that govern the observed correlations described above. In the warm climate regimes of interest to this study, the thermodynamics of H_2O have a dominant influence on the radiative feedbacks. The saturation humidity, q_s, depends exponentially on temperature as $\{e^{(-5{,}400/T)}\}/T$ (T in kelvin). As a result, a 1% increase in T from $T = 300$ K, for example, increases q_s by 17%. Indeed, satellite observations[9,10] reveal that total atmospheric water vapour increases by ~17% per 1% increase in SST. Hence G_a increases with SST.

The latent energy of a parcel of air also grows by 17% per 1% increment in T. When $T > 300$ K, a parcel of moist air near the surface has sufficient latent energy that if it is forcibly lifted until it reaches saturation, it can overcome the gravitational potential energy and rise to the upper troposphere as a cumulonimbus cloud[11,12]. The ice crystals detrained by these deep clouds spread thousands of kilometres downwind in the form of cirrus anvils[22,23] and also moisten the upper troposphere[18]. The maxima in the cloud-forcing fields (Fig. 1) are caused by the cirrus anvils[12] and not by the cumulonimbus clouds, which are two orders of magnitude smaller[23]. When SST drops below 300 K, the latent energy in the surface layer is generally not sufficient to form deep convection[24]. Hence G increases rapidly when $T > 300$ K.

Consider next the total static energy of the atmosphere, $h = C_pT + gZ + Lq$, where the first term is the thermal energy, the second is the gravitational potential energy and the third is the latent energy, with Z the altitude and q the H_2O mass mixing ratio. We rewrite it in the form $h/C_p = T + (g/C_p)Z + (L/C_p)q$ where $g/C_p = 9.8$ K km^{-1} and $L/C_p = 2{,}500$ K. At $T = 303$ K, the saturation q at the surface is 0.026, and assuming a reasonable value of 75% for the relative humidity, the latent energy is ~50 K and $h/C_p = 353$ K. If we adopt the observed equatorial temperature and humidity profiles[25], h/C_p decreases from 353 K at $Z = 0$ km to 330 K at $Z = 6$ km. Above 6 km it increases with Z to ~350 K at 16 km because of the dominance of the potential energy term. As a result, a surface parcel with SST = 303 K can penetrate to ~16 km. When the SST drops to 297 K, the surface parcel has a static energy of only 330 K and can barely reach the middle troposphere.

The warmer ocean thus produces clouds at higher altitudes. As cloud-top temperature and emission of radiation to space decrease with altitude, these clouds trap more long-wave radiation and have a larger greenhouse effect[26]. As a result C_l can increase with SST. Why does the solar reflection increase with SST? Deeper penetration by clouds is not sufficient to account for the enhanced solar reflection; in addition, the extent of cloudiness and the optical thickness of the clouds have to increase with SST. The required moisture for sustaining cirrus is not necessarily provided by local evaporation[27] but instead by large-scale transport within the lower troposphere into the region of convection[27,28]. These large circulation systems are the

'Hadley' and 'Walker' circulations[4]. The sources of energy for these large-scale motions are the latent heat released by convection[29], the cirrus long-wave cloud forcing and the spatial gradients in SST[30]. Therefore this convective large-scale system is self-sustaining. The large-scale convergence of moisture into the warm oceanic regions amplifies the warming through the enhanced atmospheric greenhouse effect, further driving the circulation. This continues until the cirrus clouds, which accumulate during this process, reflect enough sunlight to arrest further warming. Thus the anvils act like a thermostat.

Predictions of the thermostat hypothesis

The independent natural experiments support this hypothesis: the feedback between SST, convection and cloud reflection of solar radiation prevents a runaway greenhouse effect on the SST and acts as a thermostat to regulate the maximum ocean temperatures on the planet. The climate implications of this hypothesis are now developed in more detail.

Maximum ocean temperature. Let us consider an ocean region where dynamical transport of heat in the surface layers is negligible so that it can reach the maximum value imposed by the solar absorption. The equatorial western Pacific nearly satisfies this criterion because the net heat flux into the ocean is very small (0–20 W m^{-2})[31,32]. We can therefore apply equation (1) with a correction for atmospheric transport which is discussed next. An examination of the equatorial temperature gradients[25] reveals that the mid-to-upper troposphere has negligible east-west and north–south gradients in spite of the fact that the latent heating (200–300 W m^{-2})[4,31] and cloud greenhouse effect add as much as 300–400 W m^{-2} heat flux in the western portions of the Pacific. Seasonal and longitudinal average temperatures in the upper troposphere differ by less than 2 K between 25° N to 25° S. Likewise, the upper troposphere in the equatorial western Pacific is less than 2 K warmer than that of the eastern Pacific 10^4 km away. This homogeneity follows from the balancing of latent and radiative heating in the tropical atmosphere by adiabatic cooling resulting from convective and large-scale overturning[33]. In particular, adding energy to the upper troposphere is very effective in driving the Walker and the Hadley cell circulation[29]. Recent general circulation model studies[34,35] also suggest that the radiative energy converging in the anvils does not cause localized warming over the anvil regions. Instead, the warming is uniformly distributed over the entire tropical region.

We therefore assume that the C_l term, which is largely heat trapped in the troposphere, is transported out of the western Pacific, and only a small fraction contributes to warming the ocean locally. This fraction, f, ranges between 0 and 0.2. The upper bound is related to the fraction of the long-wave emission from the base of cirrus clouds that can reach the ocean surface directly. Incidentally, C_l (~60–80 W m^{-2}) is nearly equal to the net annual mean radiative heating of 80 W m^{-2} (ref. 36) at the top of the atmosphere minus the oceanic heat transport[32] of ~0–20 W m^{-2} in the western Pacific region. This implies that 60 W m^{-2} is being transported out of the region by advection within the atmosphere, which is consistent with the assumed range for f.

On the other hand, the C_s term represents a direct loss of solar energy to the ocean surface[34]. With the above inferences, equation (1) can be rephrased as follows:

$$\mathrm{SST}_{\max} = T_0 + \{(S_c + G_0 - \sigma T_0^4)/\beta\} \qquad (2)$$

$$\text{where } \beta = 4\sigma T_0^3 - \mathrm{d}G_a/\mathrm{d}T - f\,\mathrm{d}C_l/\mathrm{d}T - \mathrm{d}C_s/\mathrm{d}T$$

The net radiative feedback is denoted by β. The variables have been expanded about a reference temperature T_0; for example, $G_a = G_0 + \mathrm{d}G_a/\mathrm{d}T$, where $G_0 = 165$ W m^{-2} is the value of G_a at T_0, assumed to be 300 K. It is safe to assume an uncertainty of ~±15 W m^{-2} in the radiative flux terms. The clear-sky solar absorption is $S_c = S(1 - A_c) = 370$ W m^{-2}, where $S = 424$ W m^{-2} is the annual mean equatorial solar radiation and $A_c = 0.1$ is the clear-sky albedo, and we subtract 12 W m^{-2} for stratospheric solar absorption[37]. Similarly, the stratospheric contribution of 5 W m^{-2} to G_a has been subtracted from G_0. The values derived from Figs 3 and 4 are adopted for the various feedback terms in β. Changes in the equatorial atmospheric temperature and humidity profiles in response to SST changes are implicitly included in the long-wave feedback terms, as $\mathrm{d}G_a$ and $\mathrm{d}C_l$ are obtained directly from observed changes. The cloud feedback terms arising from convection will be zero when $T < T_0$, and the black-body term is $4\sigma T_0^3 = 6.1$ W m^{-2} K^{-1}. Note first that in the absence of the cloud feedback terms, the black-body negative feedback (the first term in the denominator) is dominated by the positive feedback effect of $\mathrm{d}G_a/\mathrm{d}T$ (6.8 W m^{-2} K^{-1}), creating a potentially unstable state. Substitution of $-27 < \mathrm{d}C_s/\mathrm{d}T < -22$ and $18 < \mathrm{d}C_l/\mathrm{d}T < 23$ yields:

$$303 < \mathrm{SST}_{\max} < 305 \text{ K}$$

The lower limit is for $f = 0.0$ and $\mathrm{d}C_s/\mathrm{d}T = -27$, and the upper limit of 305 K is for $f = 0.2$ and $\mathrm{d}C_s/\mathrm{d}T = 22$ W m^{-2} K^{-1} (from Fig. 3). If we allow 20 W m^{-2} for oceanic heat transport, the 305 K value drops to ~304 K and the 303 K value drops to 302 K in agreement with observed western Pacific SSTs (Fig. 2*a*). For the above example, the feedback value ranges between $15 < \beta < 26$ W m^{-2} K^{-1}. This large damping should tend to minimize the seasonal variations of the SST in the western Pacific.

Evaporative cooling of the warm oceans is another possible mechanism[15,25] for limiting SSTs, but this cannot be a limiting factor for several reasons: (1) the added moisture to the boundary layer will enhance G_a; and (2) observed precipitation exceeds evaporation by nearly a factor of 2 in the western Pacific[4,25,31] (the western Pacific ocean imports rather than

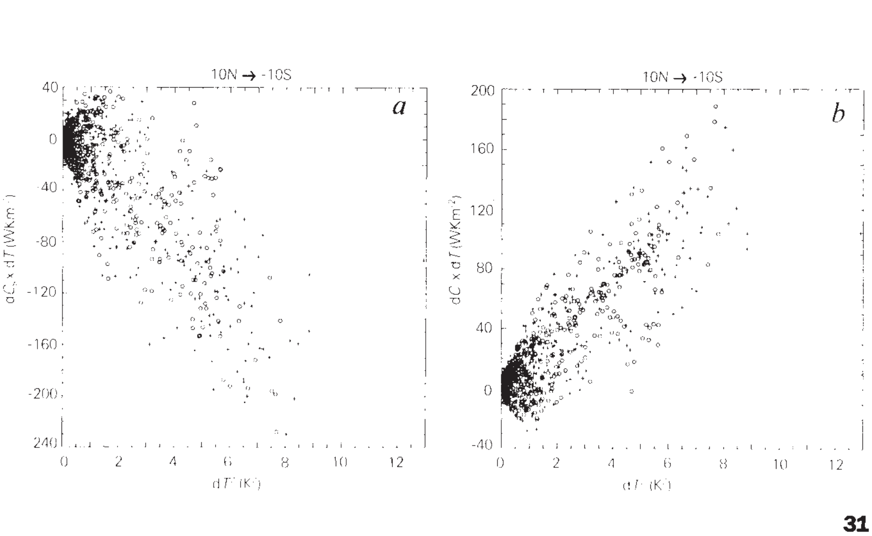

FIG. 4 *a*, Change induced by 1987 El Niño in solar absorption by the ocean-atmosphere system. Product of $\mathrm{d}C_s$ and $\mathrm{d}T$ against $(\mathrm{d}T)^2$ for the Pacific, 10° N to 10° S. The points represent the differences between 4/87 and 4/85(+) and 4/89 and 4/87(○). A negative value for the product indicates a decrease (increase) in absorbed solar energy with a warming (cooling) of the ocean. The linear fit is $\mathrm{d}C_s/\mathrm{d}T = -19$ W m^{-2} K^{-1} ($r = -0.80$). The error in SST data is 1 K, and when regions with $\mathrm{d}T < 1$ K are excluded the fit is $\mathrm{d}C_s/\mathrm{d}T = -22$ W m^{-2} K^{-1} ($r = -0.73$). *b*, Same as (*a*) but for cloud long-wave forcing. The linear fit is $\mathrm{d}C_l/\mathrm{d}T \approx 16$ and increases to 17.5 W m^{-2} K^{-1} when points with $\mathrm{d}T < 1$ K are excluded.

exports water vapour). This inference, albeit based on imprecise observations, is also substantiated by the low salinity of the surface water[31]. What is needed is a permanent loss of energy, and reflection of sunlight back to space is the most efficient mechanism to accomplish this task.

El Niño warming. The basic hypothesis should apply during an El Niño as well. Indeed, during both the 1987 El Niño and the more severe 1983 El Niño[4], the maximum SST did not exceed 303 K. In the central and eastern Pacific, upwelling of colder water from below and advection of cold water from the eastern coast causes SSTs to drop below 303 K (refs 4, 31). When the dynamical cooling effects abate during periods such as an El Niño year, the SST approaches the maximum value permitted by the anvil thermostat. Thus the El Niño year constitutes the equilibrium state of the Pacific, whereas the non El Niño years are the periods when the central and east Pacific is pulled away from equilibrium by the ocean dynamics.

Greenhouse and solar-dominated climate regimes

For the oceans[9], the globally averaged greenhouse effect (G) is 175 W m^{-2} and the absorbed solar radiation is 240 W m^{-2}. For the warmest equatorial oceans, the maximum values are $G \approx 280$ (Fig. 2*a*) and solar absorption ~300 W m^{-2} (ref. 36). In the absence of clouds, S can be as large as 380 W m^{-2} (ref. 6). Thus as the planet gets warmer, it shifts from a solar-energy-dominated regime to a regime in which the greenhouse effect becomes comparable to the solar absorption. The extreme example of this convective response to warming is Venus, with a convectively driven deep troposphere of ~60 km, overcast conditions and a high planetary albedo of 80% (compared with 30% for Earth). As a result, although Venus receives twice as much solar radiation as Earth at the top of the atmosphere, the absorbed solar radiation is smaller (~150 W m^{-2}). But in spite of this brightening effect, the planet is hotter (750 K) because its atmospheric greenhouse effect exceeds 17,000 W m^{-2}.

The feedback between convection, greenhouse effect and planetary brightness limits the temperatures in the warmest regions of the Earth to less than 305 K. What is the implication of this negative feedback if its validity extends to a perturbed atmosphere? It would take more than an order-of-magnitude increase in atmospheric CO_2 to increase the maximum SST by a few degrees, in spite of a significant warming outside the equatorial regions. In this regard, the present hypothesis departs considerably from modern general circulation models. It is encouraging, however, that some model studies[1,16] are finding a marked feedback in the thermodynamic link between SST and cirrus properties. More significantly, a recent coupled ocean-atmosphere/general circulation model study[28] has suggested that the interaction between SST and solar radiation at the ocean surface is an important negative feedback in the El Niño dynamics. This result was also indicated qualitatively by earlier studies[15,38]. For the hypothesis to become a validated theory, we need to establish the link between convection dynamics, large-scale moisture convergence into the warm regions and the brightness of those regions. Three-dimensional climate models in conjunction with detailed field and satellite observations can provide that link, but first the models must pass the test posed by the El Niño observations. □

Received 26 February; accepted 5 April 1991.

1. Mitchell, J. F. B., Senior, C. A. & Ingram, W. J. *Nature* **341**, 132-134 (1989).
2. IPCC *Climate Change* (Cambridge University Press, 1990).
3. Cess, R. D. *et al. Science* **245**, 513-516 (1989).
4. Philander, G. S. *El Niño, La Niña & the Southern Oscillation* (Academic, London, 1990).
5. Ardanuy, P. E. & Kyle, H. L. *Mon. Weath. Rev.* **114**, 415-433 (1986).
6. Harrison, E. F. *et al. J. geophys. Res.* **95**, 18687-18703 (1990).
7. Reynolds, R. W. *J. Clim.* **1**, 75-86 (1988).
8. WMO Report: *The Global Climate System 1986-1988 3rd Biennial Rev.* (CSMR 89/86 Geneva).
9. Raval, A. & Ramanathan, V. *Nature* **342**, 758-761 (1989).
10. Stephens, G. L. *J. Clim.* **3**, 634-645 (1990).
11. Betts, A. K. & Ridgway, W. *J. atmos. Sci.* **46**, 2621-2641 (1989).
12. Houze, R. A. & Betts, A. K. *Rev. Geophys. Space Phys.* **19**, 541-576 (1981).
13. Cane, M. A. & Zebiak, S. E. *Science* **228**, 1085-1087 (1985).
14. Gadgil, S., Joseph, P. V. & Joshi, N. V. *Nature* **312**, 141-143 (1984).
15. Graham, N. E. & Barnett, T. P. *Science* **238**, 657-659 (1987).
16. Somerville, R. C. & Remer, L. *J. geophys. Res.* **89**, 9668-9672 (1984).
17. Hallberg, R. thesis, Univ. of Chicago (1990).
18. Rind, D. *et al. Nature* **349**, 500-503 (1991).
19. Hallberg, R. Eureka Conf. Abstr. ENV1.1K CALTECH (Calif. Inst. Technol., Pasadena, California, 1991).
20. Cess, R. D., Briegleb, B. P. & Lian, M. S. *J. atmos. Sci.* **39**, 53-59 (1982).
21. Randel, D. L. & vonder Haar, T. H. *J. Clim.* **3**, 1168-1173 (1990).
22. Liou, K. *Mon. weath. Rev.* **114**, 1167-1199 (1986).
23. Houze, R. A. & Hobbs, P. V. *Adv. Geophys.* **24**, 225-314 (1982).
24. Fu, R., Del Genio, A. D. & Rossow, W. *J. Clim.* **3**, 1129-1152 (1990).
25. Newell, R. E. *et al. The General Circulation of the Tropical Atmosphere* Vol. 1 (MIT Press, Massachusetts, 1974).
26. Ramanathan, V. *J. atmos. Sci.* **34**, 1886-1897 (1977).
27. Cornejo-Garrido, A. G. & Stone, P. H. *J. atmos. Sci.* **34**, 1155-1162 (1977).
28. Barnett, T. P. *et al. J. Clim.* (in the press).
29. Hartmann, D. L. *et al. J. atmos. Sci.* **41**, 113-121 (1984).
30. Lindzen, R. S. & Nigam, S. *J. atmos. Sci.* **44**, 2418-2428 (1987).
31. Pickard, G. L. & Emery, W. J. *Descriptive Physical Oceanography* (Pergamon, Oxford, 1982).
32. Gent, P. R. *J. geophys. Res.* **96**, 3323-3330 (1991).
33. Holton, J. *Introduction to Dynamic Meteorology* (Academic, 1972).
34. Slingo, A. & Slingo, J. M. *Q. Jl. R. met. Soc.* **114**, 1027-1062 (1988).
35. Ramaswamy, V. & Ramanathan, V. *J. atmos. Sci.* **46**, 2293-2310 (1989).
36. Stephens, G. *et al. J. geophys. Res.* **86**, 9739-9760 (1981).
37. Ramanathan, V. & Dickinson, R. E. *J. atmos. Sci.* **36**, 1084-1104 (1979).
38. Ramanathan, V. *J. met. Soc. Japan.* spec. vol. *Short- and Medium-Range Numerical Weather Prediction*, 151-176 (1987).

ACKNOWLEDGEMENTS. We thank the NASA Langley Research Center for processing the calibrated ERBE data, and A. Heymsfield and S. Sherwood for their comments on the paper. This work is supported by NASA, NSF and the Vetlesen fund.